Image Quality Optimization and Soft Tissue Visualization in Cone-Beam CT Imaging

Aude Castonguay-Henri, Dmitri Matenine, Matthieu Schmittbuhl, and Jacques A. de Guise

Abstract

Cone Beam CT is a well-established diagnostic tool for numerous applications. While providing better spatial resolution and exposing the patient to lower radiation doses than conventional CT, it is also subject to spatially dependent bias due to the beam energy spectrum, resulting in a very limited capacity for soft-tissue and quantitative imaging. The goal of this work is to improve image contrast resolution and density quantification, to reinforce diagnosis efficiency and accuracy. An iterative polyenergetic approach is adapted to CBCT in order to reduce the artifacts caused by the beam hardening phenomenon and monoenergetic approximations at reconstruction level. It integrates the X-ray spectrum of the source and the cone-beam geometry, and is based on the Iterative Maximum-likelihood Algorithm for CT (IMPACT), which defines the energy-dependent attenuation coefficient as a linear combination of photoelectric and Compton effects. Our preliminary results demonstrate reduction of cupping and successful quantitative reconstruction of simple phantoms using simulated and experimental CBCT data.

Keywords

Cone beam CT • Iterative reconstruction • Spectral reconstruction • Soft tissue imaging

A. Castonguay-Henri (✉) · D. Matenine · M. Schmittbuhl · J. A. de Guise
Laboratoire de Recherche en Imagerie et Orthopédie, Centre de Recherche du Centre Hospitalier de L'Université de Montréal, Montréal, QC, Canada
e-mail: Aude.castonguay@gmail.com

A. Castonguay-Henri · D. Matenine · J. A. de Guise
Département de Génie de La Production Automatisée, École de Technologie Supérieure, Montréal, QC, Canada

M. Schmittbuhl
Faculté de Médecine Dentaire, Université de Montréal, Montréal, QC, Canada

1 Introduction

Cone beam computed tomography (CBCT) has recently become a leading technology in medical imaging and is gaining new applications such as ear, nose and throat imaging or osteoarticular exploration of extremities. It has proven its value in comparison with multidetector CT (MDCT) by offering radiologists high-resolution images of bony structures, while using less ionizing radiation for the patient. However, even with a better resolution than the MDCT, CBCT of dental and bony structures is subject to various artifacts arising from beam hardening, with many of the structures being composed of compact bone, and also due to routine presence of metallic dental restorations. In addition to this, CBCT suffers from artifacts due to scattered radiation, due to its large cone opening. The combination of beam hardening and scattering limits the diagnostic use for soft tissue. Therefore, improving contrast in soft tissue would lead to a low-dose and high-resolution imaging systems for a broader range of diagnostic applications.

Computed tomography imaging estimates a 3D map of *radiodensity* or radiation attenuation coefficients of the subject. The methods currently used for clinical CBCT reconstructions are usually based on filtered backprojection, like the Feldkamp, Davis and Cress (FDK) approach [1]. They have the advantage of requiring low computational resources, but rely on empirical corrections for sources of artifacts. In order to allow for accurate CBCT imaging of soft tissue, the most promising approaches are model-based iterative reconstruction algorithms [2]. Such iterative methods have the advantage over analytical ones to allow for the incorporation of prior information on the system and the imaged object. The prior information we aim to use is the emission spectrum of the source, while the attenuation model is largely based on Alvarez-Macovski decomposition [3], in order to reduce the spectral artifacts typically encountered with analytical reconstruction methods. Moreover, a quantitative imaging algorithm is desirable, so that a

L. Lhotska et al. (eds.), *World Congress on Medical Physics and Biomedical Engineering 2018*,
IFMBE Proceedings 68/1, https://doi.org/10.1007/978-981-10-9035-6_51

low bias in radiodensity estimation is ensured in the whole 3D volume. Therefore, it may become possible to visualize and eventually segment soft tissues based on their linear attenuation coefficient, and to evaluate the feasibility of accurate quantitative cone-beam imaging. The approach adapted to CBCT in this paper is the Iterative Maximum-likelihood Polychromatic Algorithm for CT (IMPACT) by De Man et al. [4]. It is to note that the goal of this paper is not to attain the high spatial resolution typically expected from CBCT systems nor to propose a fast numerical implementation, but mostly to propose a proof of concept of enhanced soft tissue imaging in CBCT.

2 Materials and Methods

2.1 Attenuation Physics

In the IMPACT algorithm selected for image reconstruction, the attenuation coefficient of each voxel is estimated iteratively by interpreting the intensity measured by the detector and comparing it with the expected intensity given the tissues and materials encountered by the photons. It therefore needs a model of attenuation adapted to the radiation source, the detector and the expected attenuating behaviour of different tissues. The selected direct model is the polychromatic Beer-Lambert attenuation law discretized over space and photon energy spectrum:

$$\hat{y}_i = \sum_k I_k E_k S_k \exp\left(-\sum_i x_{ij}\mu_j(E_k)\right), \tag{1}$$

where $\hat{y}_i$ is the expected intensity at detector bin i, I_k is the normalized intensity emitted at energy k, E_k is the energy in keV, S_k is the detector's sensitivity at energy k, x_i is the distance travelled by ray i inside voxel j in cm and $\mu_j(E)$ is the attenuation coefficient of voxel j in cm^{-1}. In this model, the emitted spectrum and the detector sensitivity may be estimated once and used as sets of constants. However, $\mu_j(E)$ depends on the subject composition, which is heterogeneous.

The definition for μ arises from modelization of the physical phenomena encountered by the x photons [2, 4, 5], as we aim to represent the CBCT system and its associated phenomena with enhanced accuracy. Three main interactions take place in kV x-ray imaging: Rayleigh scattering, Compton scattering and photoelectric absorption [6]. The first one can be omitted, as photons are scattered at low angles and do not lose energy in the process, and the interaction cross-section strongly decreases with higher energies. Compton scattering is an interaction where a photon loses energy and changes direction via an inelastic collision with an electron essentially considered free, and is prevalent in soft tissues. The photoelectric effect is the absorption of photons by ejection of bound electrons of atoms, prevalent in bones and metallic restorations [6]. The energy dependence of the photoelectric cross-section is approximated by $\Phi(E) = 1/E^3$, while Compton scattering cross-section is modelled by the Klein-Nishina function $\Theta(E) = f_{KN}(E)$ [3]. These relationships allow for estimation of relative occurrence rates of both phenomena, where photon energy is the independent variable. A second set of weighting factors is determined by the equivalent atomic number of the tissue or material. This leads to the following definition of μ:

$$\mu = \phi \cdot \Phi(E) + \theta \cdot \Theta(E), \tag{2}$$

where ϕ and θ are respectively the photoelectric effect and the Compton effect coefficients of the tissue based on a limited number of base materials. Equations (1) and (2) define the attenuation model that will be used for the reconstruction, while geometrical modelling follows Siddon's ray-tracing method, which considers a space of square voxels and infinitely thin linear x-ray attenuation paths [7].

As most iterative methods, an initial image is assumed and then modified after each iteration. We used a uniform image with $\mu = 0.1$ as initialization. The attenuation coefficient of each voxel in then associated with its Compton and photoelectric components by interpolating on the $\phi(\mu)$ and $\theta(\mu)$ curves drawn with the values shown in Table 1, proposed by De Man [4].

Projections of the estimated image are calculated based on Eqs. (1) and (2), and are then used to determine the correction $\Delta\mu_j^n$ needed for voxel j at iteration n. The objective function to maximize is the log-likelihood L:

$$L = \sum_{i=1}^{I} (y_i \cdot \ln(\hat{y}_i^n) - \hat{y}_i^n), \tag{3}$$

where y_i is the measured intensity at detector bin i. the maximum-likelihood algorithm for transmission tomography (ML-TR) [8] was employed to maximize Eq. (3). We applied a 3×3 median filter on the image every 10 iterations to reduce aliasing artifacts.

Table 1 Attenuation coefficients at 70 keV and associated Compton and photoelectric coefficient for common substances

Substances	θ (1/cm)	ϕ (1/cm)	μ (1/cm)
Air	0.0002	1.7e−05	0.0002
Soft tissue	0.1777	0.0148	0.1935
Water	0.1783	0.0144	0.1946
Aluminium	0.4274	0.2125	0.6523
Iron	1.3904	5.32734	7.0748

2.2 Experiments

Our main hypothesis states that the reduction of beam hardening artifacts will enhance the contrast in CBCT imaging. We therefore tested our algorithm on numerical and physical phantoms in order to observe the impact of polychromatic iterative reconstruction on the cupping artifact. Those images were compared with a monochromatic iterative method, the ordered subsets convex algorithm with total variation regularization (OSC-TV) proposed by Matenine et al. [9], as well as with FDK. The latter was implemented using the OpenRTK library [10] and OSC-TV was implemented in-house using C++. IMPACT was implemented using Matlab®. Two types of input sets of projections or *sinograms* were used: simulated and real.

Two different phantoms were reconstructed using experimental projection data. The water phantom was a thin-walled plastic cylinder filled with tap water and a diameter of 8 cm. It was used to observe the algorithm's effect on the cupping artifact. The polytetrafluoroethylene (PTFE) wedge phantom was similar in construction to the water phantom, with a water cylinder of 11 cm in diameter and a quarter-disk PTFE insert held in place by a thin polymethyl methacrylate (PMMA) plate. It was used to analyse the capacity for quantitative imaging of highly attenuating objects. The expected profiles were estimated with data from the *XCOM* database [11].

A simulated sinogram of the wedge phantom was acquired via Siddon's ray-tracing in a voxelized numerical phantom of equal dimensions, using attenuation coefficients for photon energies from 1 to 110 keV with increments of 1 keV, retrieved from the *XCOM* database for the materials of interest. Matlab was used for the numerical implementation. This allowed us to compare reconstructed images based on simulated projections with the physical phantom reconstructions and in turn compare quantification accuracy. It is important to notice that simulated sinograms did not include scatter readings, while real sinograms were affected by scatter. Comparison of reconstructions of simulated and real sinograms permitted to quantify bias due to scattered radiation. Real projections were acquired with the NewTom 5G (Verona, Italy) cone beam CT scanner, see Table 2 for acquisition parameters.

The x-ray source spectrum used for simulated scans was generated at 1 keV increments using the SRS-78 application [12], which uses the scanner tube anode angle, filtration and peak voltage (kVp) as inputs. The same estimated spectrum was used in the IMPACT reconstruction algorithm, with a more coarse discretization over 20 energy bins. The detector sensitivity profile was considered uniform with respect to photon energy for the simulated and real data studies.

Table 2 Real sinogram CBCT acquisition protocols and corresponding image pixel sizes for reconstructed slices. The slice thickness is equal to the pixel side

Experiment	FOV: diameter (cm) × axial coverage (cm)	Reconstructed pixel size (mm × mm)
Water phantom	8 × 8	1.5 × 1.5
Wedge phantom	15 × 5	0.6 × 0.6

The central slice was reconstructed using FDK, OSC-TV and IMPACT. Still, the cone beam collimation was that of clinical CBCT protocols and scattered radiation contributed to the central slice sinogram. Line profiles of the reconstructed slice were acquired on the central sagittal axis in order to evaluate cupping. For the water phantom, cupping was quantified by computing a polynomial fit on the part of the profile which represents water only, using the model below:

$$\mu(x) = a(x-b)^2 + c, \tag{4}$$

where a is the coefficient which increases with increasing cupping and b, c are translation parameters. The bias on μ was quantified on a circular region of interest (ROI), centered on a uniform region of the phantom and excluding borders. Mean value and standard deviation of μ over the ROI were calculated. The μ values were compared for a reference energy of 70 keV, which, in a clinical setting, ensures a good contrast between soft and bony tissues.

3 Results

3.1 Water Phantom

Figure 1 shows profiles and images for a real water cylinder reconstruction with IMPACT, OSC-TV and FDK. The polynomial fit led to $a = (1.31 \pm 0.16) \times 10^{-5}$ for IMPACT, $a = (2.28 \pm 0.10) \times 10^{-5}$ for OSC-TV and $a = (3.2 \pm 1.0) \times 10^{-5}$ for FDK. This indicates that the monochromatic approaches suffer from more severe cupping than IMPACT.

The mean and standard deviation in the circular ROI inform us on the bias in the image. Higher values of standard deviation indicate that the attenuation coefficients are held within a larger range of values, which includes noise and spatially-dependent bias. Figure 2 shows the analysis of all the water voxels of the water cylinder phantom, excluding borders, for each method. On a relative scale, we observe a $(2.5 \pm 0.9)\%$ μ bias for IMPACT, $(12 \pm 2)\%$ for OSC-TV

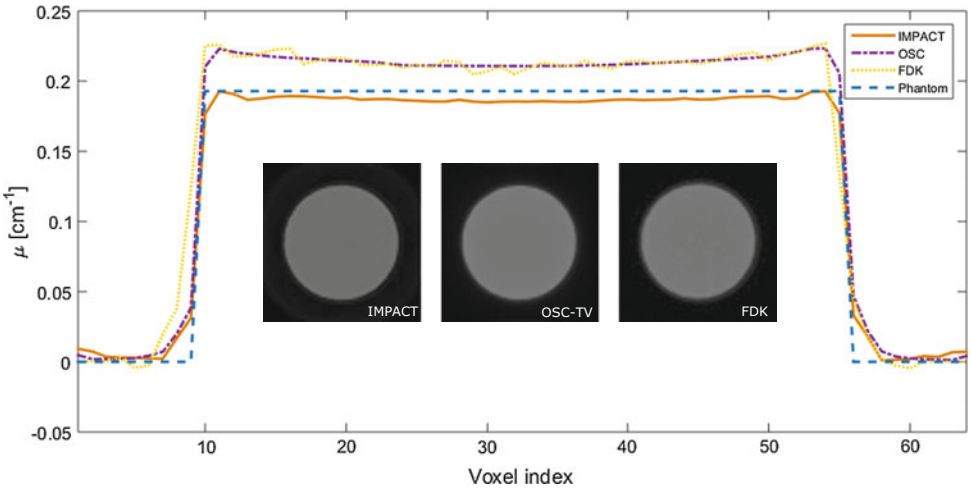

Fig. 1 Reconstruction of the central slice of the real water phantom and μ for each voxel along the central line of the image. Some cupping is present in the IMPACT reconstruction, likely due to scattered radiation, but more accurate attenuation coefficients are obtained

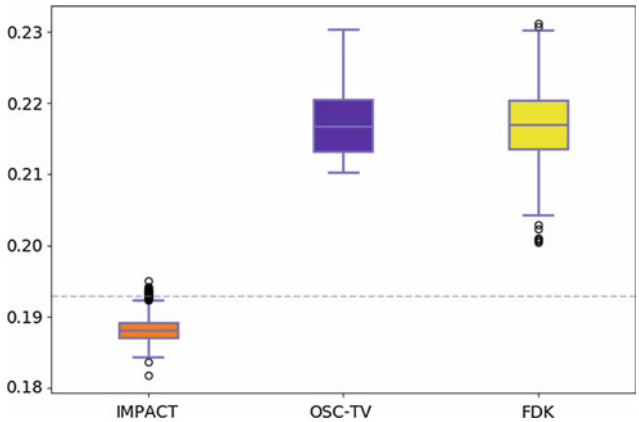

Fig. 2 Analysis of reconstructed water phantom attenuation coefficient for each method. IMPACT leads to more accurate and more precise values. The dashed line represents the ground truth

and (12 ± 2)% for FDK, when compared to the ground truth. In general, we observe that monochromatic approaches yield a systematically higher μ estimate and suffer from severe cupping, while IMPACT yields a more uniform profile closer to the expected value. The remaining cupping for IMPACT is likely due to scattered radiation, which also causes cupping.

3.2 Wedge Phantom

Figure 3 shows the reconstructions of the wedge phantom. While OSC-TV and FDK seem to lead to very similar images, IMPACT reconstructions show lower contrast between the water and the PTFE. This is explained by the lower μ calculated with IMPACT for PTFE, as shown by the profiles in Fig. 4a, b. The bias values were also calculated in circular regions of interest excluding borders for PTFE.

For the simulated phantom, a (0.6 ± 1.0)% μ bias was observed for IMPACT, (32 ± 3)% for OSC-TV and (32 ± 3)% for FDK in the wedge region. The lower standard deviation for IMPACT still indicates a reduction in cupping, in addition to the visual aspect of the profiles. Moreover, we observe an important reduction of streak artifacts with IMPACT, compared to FDK.

For the real wedge phantom, the μ bias in the wedge region was of (11 ± 1)% for IMPACT, (3 ± 3)% for OSC-TV and (3 ± 4)% for FDK. The reconstructed μ are closer to the phantom's values with OSC-TV and FDK for the central region, but cupping is prominent on the edge of the phantom. IMPACT yields a systematic under-estimation of the profile, but a successful cupping correction.

4 Discussion and Conclusions

IMPACT shows definitive potential for both quantitative reconstruction and cupping reduction. The latter was reduced in all cases, simulated and real. Discrepancies between reconstruction of simulated and real projections give us indications as to how well the system is modelled. The main difference is that scattered radiation was not considered, but only beam hardening artifacts were. In consequence, IMPACT seems to interpret scatter signal as beam hardening, so the reconstructed profiles are relatively flat, but are somewhat biased. Another source of bias is the detector sensitivity profile. It is currently approximated as a constant for lack of an experimentally obtained sensitivity profile. An additional source of bias is the emission spectrum, which was estimated instead of being measured for the individual x ray tube. Having the individual emission spectrum could lead to a better estimation of polychromatic phenomena, and therefore more accurate values of linear attenuation coefficients. It should be noted that even though the simulations were performed in 2D, experimental projection data were affected by substantial

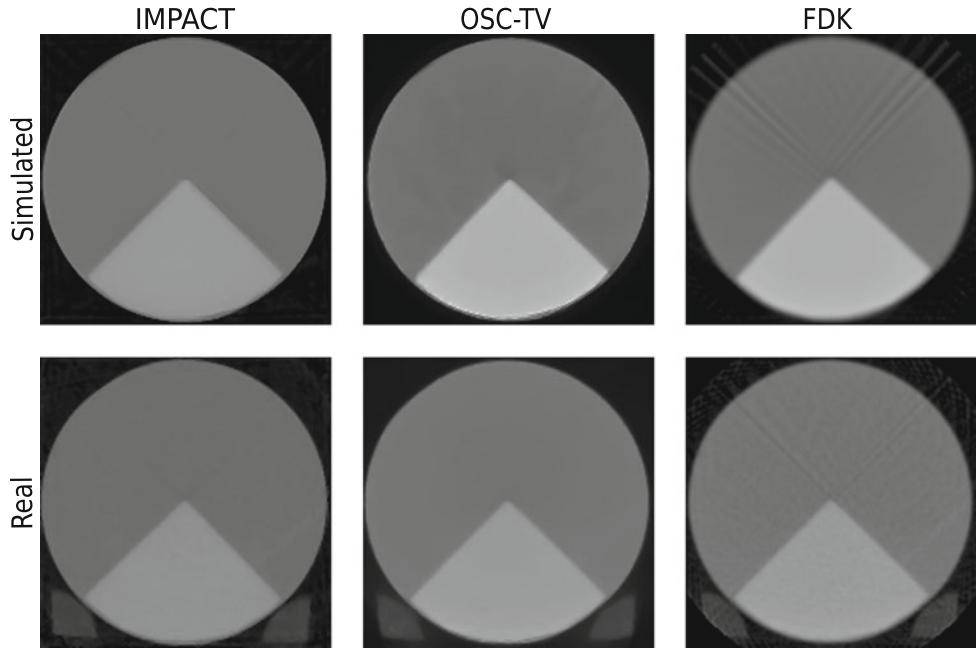

Fig. 3 Comparison of both simulated and real wedge phantoms, reconstructed using IMPACT, OSC-TV and FDK. Reduced streaking was observed for IMPACT

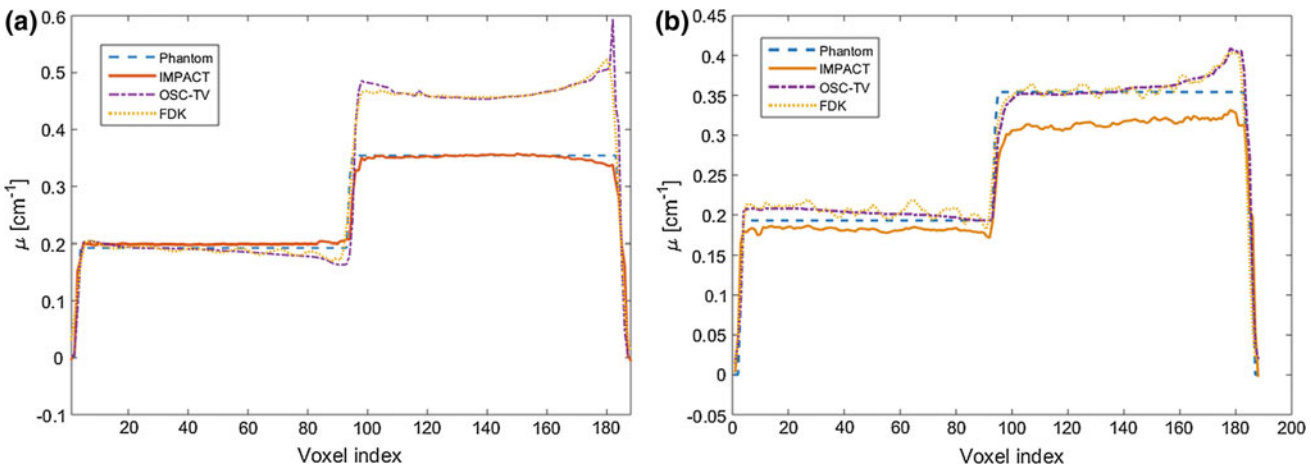

Fig. 4 Profiles of the reconstructed wedge phantoms. An important difference regarding cupping between the monochromatic and polychromatic methods was observed with both **a** simulated and **b** experimental sinograms

scatter and the final results are representative of accuracy attainable by IMPACT in CBCT.

The next step will be to evaluate the behaviour of IMPACT with respect to more complex objects, including anatomical phantoms, and implement a practical scatter correction. In order to handle larger amounts of data, a parallel implementation of IMPACT is envisioned.

Acknowledgements This work was partly financially supported by Mitacs through the Mitacs Accelerate program and by Canada Research Chairs. The authors would like to thank Useful Progress Service Inc. (Montreal, QC) and its founder Francis Siguenza for financially supporting the Mitacs Program.

Conflicts of Interest Dmitri Matenine is an employee of Useful Progress Services Inc. (Montreal, QC). Other authors declare that they have no conflict of interest.

References

1. Feldkamp, L.A., Davis, L.C., Kress, J.W. (1984). Practical cone-beam algorithm. J. Opt. Soc. Am. A, 1(6). doi:https://doi.org/10.1364/josaa.1.000612.
2. Nuyts, J., De Man, B., Fessler, J.A., Zbijewski, W., Beekman, F. J. (2013). Modelling the physics in the iterative reconstruction for transmission computed tomography. Physics in Medicine and Biology, 58(12). doi:https://doi.org/10.1088/0031-9155/58/12/r63.
3. Alvarez, R.E., Macovski, A. (1976). Energy-selective reconstructions in X-ray computerized tomography. Physics in Medicine and Biology, 21(5). doi:https://doi.org/10.1088/0031-9155/21/5/002.
4. De Man, B. et al. (2001). An Iterative Maximum-Likelihood Polychromatic Algorithm for CT. IEEE Transactions on Medical Imaging, 20(10), 999-1008. doi:https://doi.org/10.1109/42.959297.
5. Beister, M., Kolditz, D., Kalender, W.A. (2012). Iterative reconstruction methods in X-ray CT. Physica Medica, 28(2). doi:https://doi.org/10.1016/j.ejmp.2012.01.003.
6. Bushberg, J.T., Seibert, J.A., Leidholdt, E.M., Boone, J.M. (2012). The Essential Physics of Medical Imaging, 3rd edition. Lippincott Williams & Wilkins, Philadephia, USA. isbn: 978-0-7817-8057-5.
7. Siddon, R. (1985). Fast calcuation of the exact radiological path for 3-D CT. Medical Physics, 12(2). doi:https://doi.org/10.1118/1.595715
8. J. Nuyts, B. De Man, P. Dupont, M. Defrise, P. Suetens, and L. Mortelmans. (1998). Iterative reconstruction for helical CT: A simulation study. Phys. Med. Biol., vol. 43, pp. 729737.
9. Matenine, D., Mascolo-Fortin, J., Goussard, Y. & Després, P. (2015). Evaluation of the OSCTV iterative reconstruction algorithm for cone-beam optical CT. Medical Physics, 42(6376). doi:https://doi.org/10.1118/1.4931604.
10. S. Rit, M.V. Oliva, S. Brousmiche, R. Labarbe, D. Sarrut, and G. C. Sharp. (2014). The Reconstruction Toolkit (RTK), an open-source cone-beam CT reconstruction toolkit based on the Insight Toolkit (ITK). Journal of Physics: Conference Series, 489 (1).
11. Berger, M.J., Hubbell, J.H., Seltzer, S.M., Chang, J., Coursey, J.S., Sukumar, R., Zucker, D.S., and Olsen, K. (2010), XCOM: Photon Cross Section Database (version 1.5). [Online] Available: http://physics.nist.gov/xcom [2018, January 25]. National Institute of Standards and Technology, Gaithersburg, MD.
12. K. Carney, B. J. Gilmore, G. W. A. Fogarty and L. Desponds. (1997). Catalogue of Diagnostic X-ray Spectra and Other Data: Report No 78, Institute of Physics and Engineering in Medicine.
13. Hsieh, J. (2009). Computed Tomography: Principles, Design, Artifacts, and Recent Advances (2e dition). SPIE Press.